Available online at www.sciencedirect.com
SCIENCE DIRECT
Remote Sensing of Environment 99 (2005) 357 – 371
Remote Sensing of Environment
www.elsevier.com/locate/rse

Estimating light absorption by chlorophyll, leaf and canopy in a deciduous broadleaf forest using MODIS data and a radiative transfer model

Qingyuan Zhang [a,*], Xiangming Xiao [a], Bobby Braswell [a], Ernst Linder [b], Fred Baret [c], Berrien Moore III [a]

[a] Institute for the Study of Earth, Oceans and Space, University of New Hampshire, Durham, NH 03824, United States
[b] Department of Mathematics and Statistics, University of New Hampshire, Durham, NH 03824, United States
[c] Institut National de la Recherche Agronomique, Site Agroparc, 84914 Avignon, France

Received 18 January 2005; received in revised form 17 September 2005; accepted 17 September 2005

Abstract

In this paper, we present a theoretical and modeling framework to estimate the fractions of photosynthetically active radiation (PAR) absorbed by vegetation canopy ($FAPAR_{canopy}$), leaf ($FAPAR_{leaf}$), and chlorophyll ($FAPAR_{chl}$), respectively. $FAPAR_{canopy}$ is an important biophysical variable and has been used to estimate gross and net primary production. However, only PAR absorbed by chlorophyll is used for photosynthesis, and therefore there is a need to quantify $FAPAR_{chl}$. We modified and coupled a leaf radiative transfer model (PROSPECT) and a canopy radiative transfer model (SAIL-2), and incorporated a Markov Chain Monte Carlo (MCMC) method (the Metropolis algorithm) for model inversion, which provides probability distributions of the retrieved variables. Our two-step procedure is: (1) to retrieve biophysical and biochemical variables using coupled PROSPECT+SAIL-2 model (PROSAIL-2), combined with multiple daily images (five spectral bands) from the Moderate Resolution Imaging Spectroradiometer (MODIS) sensor; and (2) to calculate $FAPAR_{canopy}$, $FAPAR_{leaf}$ and $FAPAR_{chl}$ with the estimated model variables from the first step. We evaluated our approach for a temperate forest area in the Northeastern US, using MODIS data from 2001 to 2003. The inverted PROSAIL-2 fit the observed MODIS reflectance data well for the five MODIS spectral bands. The estimated leaf area index (LAI) values are within the range of field measured data. Significant differences between $FAPAR_{canopy}$ and $FAPAR_{chl}$ are found for this test case. Our study demonstrates the potential for using a model such as PROSAIL-2, combined with an inverse approach, for quantifying $FAPAR_{chl}$, $FAPAR_{leaf}$, $FAPAR_{canopy}$, biophysical variables, and biochemical variables for deciduous broadleaf forests at leaf- and canopy-levels over time.

Keywords: MODIS; PROSPECT; SAIL-2; FAPAR; Markov Chain Monte Carlo (MCMC) method

1. Introduction

Gross primary production (GPP) is a key terrestrial ecophysiological process that links atmospheric composition and vegetation processes. One of the most important of these processes, plant photosynthesis, requires solar radiation in the 0.4–0.7 μm range (also known as photosynthetically active radiation or PAR), water, carbon dioxide (CO_2), and nutrients. The fraction of PAR absorbed by the vegetation canopy ($FAPAR_{canopy}$) is therefore an important biophysical variable and is widely used in satellite-based Production Efficiency Models (Potter et al., 1993; Prince & Goward, 1995; Ruimy et al., 1996; Running et al., 2004) to estimate GPP or net primary production (NPP). In remote sensing studies, $FAPAR_{canopy}$ is usually estimated as a linear or non-linear function of Normalized Difference Vegetation Index (NDVI) (Prince & Goward, 1995; Tucker, 1979). $FAPAR_{canopy}$ is also related to leaf area index (LAI), and is estimated as a function of LAI and a light extinction coefficient in a number of process-based biogeochemical models (Ruimy et al., 1999). The LAI-$FAPAR_{canopy}$ and NDVI-$FAPAR_{canopy}$ relationships have been the dominant paradigm in the literature for estimating GPP and NPP of terrestrial vegetation at various spatial scales (Field et al., 1995; Running et al., 2004).

* Corresponding author. Complex Systems Research Center, Institute for the Study of Earth, Oceans and Space, University of New Hampshire Durham, NH 03824, United States. Tel.: +1 603 862 0019.
E-mail address: qzhang@eos.sr.unh.edu (Q. Zhang).

0034-4257/$ - see front matter © 2005 Elsevier Inc. All rights reserved.
doi:10.1016/j.rse.2005.09.009

A vegetation canopy is composed primarily of photosynthetically active vegetation (PAV) and non-photosynthetic vegetation (NPV; e.g., senescent foliage, branches and stems). The presence of NPV has a significant effect on $FAPAR_{canopy}$. For example, in forests with an LAI less than 3.0, an earlier study (Asner et al., 1998) found that stems increased canopy FAPAR by 10–40%. There is then, in principal, a need to partition $FAPAR_{canopy}$ into the fractions of PAR absorbed by green leaves and by NPV.

Furthermore, it is important to note that a green leaf is composed of chlorophyll and various proportions of non-photosynthetic components (e.g., other pigments in the leaf, primary/secondary/tertiary veins, and cell walls). Non-photosynthetic absorption in PAR wavelengths can vary in magnitude (e.g., 20–50%) among different species, leaf morphology, leaf age and growth history (Hanan et al., 1998, 2002; Lambers et al., 1998). We argue that $FAPAR_{canopy}$ should be partitioned into the fractions of PAR absorbed by chlorophyll ($FAPAR_{chl}$) and by NPV ($FAPAR_{NPV}$, including all the non-chlorophyll pigments in leaf, cell walls, veins, branches and stems).

Only the PAR absorbed by chlorophyll (a product of $FAPAR_{chl} \times PAR$) is used for photosynthesis. Therefore, remote sensing driven biogeochemical models that use $FAPAR_{chl}$ in estimating GPP are more likely to be consistent with plant photosynthesis processes (Xiao et al., 2004a,b). It is important to understand to what extent $FAPAR_{canopy}$ can be partitioned into $FAPAR_{chl}$ and $FAPAR_{NPV}$ given imperfect models and data. In an earlier study (Depury & Farquhar, 1997), a process-based leaf photosynthesis model estimated PAR effectively absorbed by PSII system per unit leaf area. However, the partitioning issue has not been studied extensively in both remote sensing and ecological communities that focus on large scales.

Quantifying the temporal evolution of $FAPAR_{chl}$ for a forest ecosystem represents an important challenge for remote sensing and ecology researchers, as it is extremely difficult to directly measure $FAPAR_{chl}$ and $FAPAR_{NPV}$ at the leaf and canopy levels on large scales over plant growing seasons. To our knowledge, no field and laboratory experiments to measure $FAPAR_{chl}$ at the leaf and canopy levels over plant growing seasons have been reported, and similarly we found no published efforts to calculate $FAPAR_{chl}$ with physics-based radiative transfer models.

In this study, we aim to develop a theoretical and technical framework for quantifying and evaluating the fractions of PAR absorbed by chlorophyll, leaf and canopy. The specific objectives of this study are twofold: (1) to clarify the concepts of $FAPAR_{chl}$, $FAPAR_{leaf}$ and $FAPAR_{canopy}$; (2) to explore the potential of estimating $FAPAR_{canopy}$, $FAPAR_{leaf}$ and $FAPAR_{chl}$, using a coupled leaf-canopy radiative transfer model with multiple daily images from the MODerate resolution Imaging Spectroradiometer (MODIS) onboard NASA Terra satellite. We used a coupled leaf-canopy radiative transfer model (PROSPECT model + SAIL-2 model) to calculate $FAPAR_{chl}$, $FAPAR_{canopy}$ and $FAPAR_{leaf}$. These models have been discussed extensively in the published literature, both separately and in combination (Bacour et al., 2002; Baret & Fourty, 1997; Braswell et al., 1996; Combal et al., 2002; Di Bella et al., 2004; Gond et al., 1999; Jacquemoud & Baret, 1990; Jacquemoud et al., 1996, 2000; Kuusk, 1985; Verhoef, 1984, 1985; Verhoef & Bach, 2003; Weiss et al., 2000; Zarco-Tejada et al., 2003). As a case study, we selected a deciduous broadleaf forest at the Harvard Forest in Massachusetts, USA, where earlier studies reported field-based observations of leaf chlorophyll content (Waring et al., 1995) and LAI (Cohen et al., 2003; Xiao et al., 2004b). This radiative transfer based modeling exercise will help us to address an important scaling issue—light absorption from chlorophyll to leaf and to canopy. Our analysis also provides guidance for designing and conducting field measurement and observations of forest canopies in the near future.

2. Description of the radiative transfer model and the inversion algorithm

2.1. Brief description of the PROSPECT + SAIL-2 model

The PROSPECT model is a leaf radiative transfer model. Previous studies used the PROSPECT model with four variables—leaf internal structure variable (N), leaf chlorophyll content (C_{ab}), leaf dry matter content (C_m), and leaf water thickness (C_w) (Demarez et al., 1999; Hosgood et al., 1995; Jacquemoud & Baret, 1990; Newnham & Burt, 2001). A number of other studies used the PROSPECT model with five variables—leaf internal structure variable (N), leaf chlorophyll content (C_{ab}), leaf dry matter content (C_m), leaf water thickness (C_w) and leaf brown pigment (C_{brown}) (Baret & Fourty, 1997; Di Bella et al., 2004; Verhoef & Bach, 2003). We used the five-variable PROSPECT model in this study because the addition of brown pigment is useful for discriminating between photosynthetic and non-photosynthetic light absorption.

The SAIL (Scattering from Arbitrarily Inclined Leaves) model is a canopy radiative transfer model. The SAIL model has been developed by several earlier researchers, evolving gradually over time with minor changes reflecting individual study objectives (e.g., Andrieu et al., 1997; Badhwar et al., 1985; Braswell et al., 1996; Goel & Deering, 1985; Goel & Thompson, 1984; Jacquemoud et al., 2000; Kuusk, 1985; Major et al., 1992; Verhoef, 1984, 1985). In this study we used the version of SAIL presented by Braswell et al. (SAIL-2; Braswell et al., 1996). The SAIL-2 model decomposes a vegetation canopy into stems and leaves. In a typical parameterization, stems have spectral properties that are more similar to soil and litter than leaves. Leaf and stem mean inclination angles and the self-shading effect of both leaves and stems are also considered.

In this study, we coupled the modified PROSPECT model with the SAIL-2 model (hereafter called PROSAIL-2) by replacing the leaf reflectance component in the SAIL-2 model with the five-variable PROSPECT model. The coupled PROSAIL-2 model was used to describe optical characteristics (reflectance, absorption and transmittance) of the canopy and its components. The PROSAIL-2 model has three groups of variables: (1) observation viewing geometry variables; (2) an

atmospheric condition (visibility) variable; and (3) biophysical and biochemical variables (Table 1). Table 1 lists the search ranges of the sixteen biophysical/biochemical variables, based on an extensive literature review. The sixteen biophysical and biochemical variables are plant area index (PAI), stem fraction (SFRAC), cover fraction (CF), stem inclination angle (STINC), stem BRDF effect variable (STHOT), leaf inclination angle (LFINC), leaf BRDF effect variable (LFHOT), five leaf variables that simulate leaf optical properties (N, C_{ab}, C_m, C_w, C_{brown}), two soil/litter variables that simulate soil/litter optical properties ($SOIL_A$, $SOIL_B$), and two stem variables that simulate stem optical properties ($STEM_A$, $STEM_B$). Because the MODIS data used in the study were atmospherically corrected, we set the atmospheric visibility variable (VIS, in Table 1) to be large and constant throughout this analysis.

2.2. Description of inversion algorithm—the Metropolis algorithm

Inversion of a radiative transfer model is computationally intensive and requires careful choices of optimization procedures. Iterative steepest-descent optimization procedures, the most commonly used approaches to invert radiative transfer models (e.g., Bacour et al., 2002), were not used in this study. These procedures are local optimization techniques with limited potential to locate globally optimal solutions. For example, if there are a few minimum points within a search space, the iterative procedures could offer a local extreme-point solution and might fail to provide a global extreme-point solution given an initial guess. As an alternative, a method based on the Metropolis algorithm (Braswell et al., 2005; Hurtt & Armstrong, 1996; Metropolis et al., 1953) was employed. This method estimates posterior probability distributions of the variables and thus can provide estimates of uncertainty (such as standard deviations and confidence intervals) of individual variables, by inspection of the retrieved distributions. The Metropolis algorithm is relatively computationally intensive, owing to the need for simulation of a large number of samples required to obtain a reliable estimate of the variables' distributions.

The Metropolis algorithm (Metropolis et al., 1953) is a type of Markov Chain Monte Carlo (MCMC) estimation procedure. At each step out of a predetermined number of iterations, the algorithm uses the current variable estimate to randomly generate a new "proposal" estimate in variable space. This new variable estimate will be the input for a new model run. Model-retrieved and observed reflectance values are used to calculate the likelihood of an error probability model. The Metropolis algorithm then accepts the new variable estimate with a certain probability. The resulting Markov Chain of accepted variable values converges to the posterior distribution of the variables conditional on the observations after a transient "burn-in" period. MCMC theory assures that such a sampling scheme provides Markov chains whose values represent draws from the posterior distributions. In the following formalism, Pr(·) denotes probability in a general sense, or more specifically, the value of a probability density function. Pr(v) denotes the prior distribution assumed for the set of variables. Pr(v_{new}|data) and Pr(v_{old}|data) refer to the conditional probabilities of "new" and "old" variable estimates (variable points) given the known "data".

According to Bayes' theorem,

$$Pr(v|data) \propto Pr(v)Pr(data|v)$$

Let $L(v) = \Pr(\text{data}|v)$

$$Pr(v|data) \propto Pr(v)L(v)$$

where $L(\cdot)$ is the likelihood function. In this study we assume a set of independent uniform prior distributions for the variables. Let $X_i = [x_{i1}, \ldots, x_{ip}]'$ ($p > 1$), i is the subscript of data point, subscripts 1, …, p mean spectral bands, and x is reflectance.

This study assumes that the observed spectral values X_i differ from the model predicted values $U_i = [u_{i1}, \ldots, u_{ip}]$

Table 1
A list of variables in the PROSAIL-2 model and their search range

	Variable	Description	Unit	Search range
Biophysical/biochemical variables	PAI	plant area index, i.e., leaf+stem area index		1–7.5
	SFRAC	Stem fraction		0–1
	CF	Cover fraction: area of land covered by vegetation/ total area of land		0.5–1
	C_{ab}	Leaf chlorophyll $a+b$ content	μg/cm^2	0–80
	N	Leaf structure variable: measure of the internal structure of the leaf		1.0–4.5
	C_w	Leaf equivalent water thickness	cm	0.001–0.15
	C_m	Leaf dry matter content	g/cm^2	0.001–0.04
	C_{brown}	Leaf brown pigment content		0.00001–8
	LFINC	Mean leaf inclination angle	degree	10–89
	STINC	Mean stem inclination angle	degree	10–89
	LFHOT	Leaf BRDF variable: length of leaf/ height of vegetation		0–0.9
	STHOT	Stem BRDF variable: length of stem/height of vegetation		0–0.9
	$STEM_A$	Stem reflectance variable: maximum (for a fitted function)		0.2–20
	$STEM_B$	Stem reflectance variable range (for same fitted function)		50–5000
	$SOIL_A$	Soil reflectance variable: maximum (for a fitted function)		0.2–20
	$SOIL_B$	Soil reflectance variable: range (for same fitted function)		50–5000
Atmospheric condition variable	VIS	Diffuse/ direct variable: scope of atmospheric clarity	km	50

according to a mean zero p-variate Gaussian error model that results in the likelihood function

$$L = \prod_{i=1}^{n} \frac{1}{\left(\sqrt{2\pi}\right)^{p} \left|\sum\right|^{1/2}} e^{-(X_i-U_i)' \sum^{-1} (X_i-U_i)/2}, \quad (1)$$

where n is the number of data points and $\sum$ is the variance–covariance matrix of X. $\sum$ is estimated by the usual sample variances and covariances in each step of the algorithm:

$$\Sigma_e = \left(S_{ij}\right)_{p\times p} \qquad i,j = 1, \ldots, p$$
$$S_{ij} = \frac{1}{n}\sum_{k=1}^{n}\left(x_{ki} - u_{ki}\right)\left(x_{kj} - u_{kj}\right). \quad (2)$$

The natural logarithm of the likelihood, the "log-likelihood" (log(L)), is used in the algorithm during its operation(e.g., Bishop, 1995).

The algorithm defines the probability to accept the new point as following:

$$Pr_{\text{accept}} = \min\left(1, \frac{Pr(v_{\text{new}}|data)}{Pr(v_{\text{old}}|data)}\right). \quad (3)$$

If the algorithm accepts the new point, it will become the "old" point in next iteration; otherwise, the old point will still be the "old" point in next iteration.

To accelerate the speed of convergence of the Metropolis algorithm, we modified the adaptive algorithm used in other studies (e.g., Braswell et al., 2005; Hurtt & Armstrong, 1996) as follows.

In each iteration, one variable is selected to change as

$$v_{\text{new},s} = v_{\text{old},s} + r \times \left(v_{\max,s} - v_{\min,s}\right) \quad (4)$$

where $s = 1, \ldots, 16$, is the number of variables in PROSAIL-2 model that are allowed to search for solutions, r is randomly selected at each step between $\pm 0.5 \cdot T_s$, $v_{\max,s}$ and $v_{\min,s}$ are the maximum and minimum values allowed to search, and T_s is temperature. If $v_{\text{new},s}$ is accepted, then T_s is increased by a factor of 1.006569. If it is rejected, then T_s is decreased by a factor of 0.99. By changing the *temperatures* in this way, the T_s ($s = 1, \ldots, 16$) of all variables are adjusted until varying any given variable leads to acceptance of about 23–44% of the time, which is considered an ideal acceptance rate for the Metropolis algorithm (Gelman et al., 2000).

2.3. Calculation of $FAPAR_{canopy}$, $FAPAR_{leaf}$, and $FAPAR_{chl}$

To calculate $FAPAR_{chl}$, $FAPAR_{leaf}$ and $FAPAR_{canopy}$ using the PROSAIL-2 model, we need to know the values of the input variables used in the model. Our strategy is to first invert the biophysical and biochemical variables using the coupled PROSAIL-2 model with observed spectral reflectance data (reflectance plus relative observation geometry), and then to calculate $FAPAR_{chl}$, $FAPAR_{leaf}$ and $FAPAR_{canopy}$ using forward simulations.

We calculated $FAPAR_{canopy}$ (Goward & Huemmrich, 1992), $FAPAR_{leaf}$ (Braswell et al., 1996), and $FAPAR_{chl}$ (see Eqs. (5)–(9)) using the PROSAIL-2 model with the variable values from the inversion.

$$\text{FAPAR}_{\text{canopy}} = \frac{\text{APAR}_{\text{canopy}}}{\text{PAR}_0} \quad (5)$$

$$\text{FAPAR}_{\text{leaf}} = \frac{\text{APAR}_{\text{leaf}}}{\text{PAR}_0} \quad (6)$$

$$\text{FAPAR}_{\text{chl}} = \frac{\text{APAR}_{\text{chl}}}{PAR_0} \quad (7)$$

$$\text{APAR}_{\text{canopy}} = \text{APAR}_{\text{leaf}} + \text{APAR}_{\text{stem}} \quad (8)$$

$$\text{APAR}_{\text{leaf}} = \text{APAR}_{\text{chl}} + \text{APAR}_{\text{dry matter}} + \text{APAR}_{\text{brown pigment}} \quad (9)$$

where PAR_0 is the incoming PAR at the top of the canopy, and APAR is the absorbed PAR. $APAR_{canopy}$, $APAR_{leaf}$, $APAR_{stem}$, $APAR_{chl}$, $APAR_{dry\ matter}$, and $APAR_{brown\ pigment}$ are absorbed PAR by canopy, leaf, stem, chlorophyll in leaf, dry matter in leaf, and brown pigment in leaf, respectively.

2.4. Inversion of the PROSAIL-2 model with simulated data

After integration of the coupled PROSAIL-2 model with the Metropolis inversion algorithm, we conducted a number of model inversion runs with simulated data to examine the performance of the modeling framework. Here we report results from one typical group of these model-simulated data (Table 2). We used the values of individual variables in Table 2 to simulate reflectance as the first simulated data set. For the second simulated data set, we added random noise (mean = 0, standard deviation = 5% of reflectance) to represent error in the reflectance prior to inversion. In the third simulated data set, we added a different amount of random noise (mean = 0, standard deviation = 10% of reflectance) to the reflectance. Inversion of the PROSAIL-2 model was conducted for the three simulated data sets, using the MCMC algorithm (see Section 2.2). All the sixteen variables (Table 1) were estimated simultaneously for the three simulated data sets.

The strength of the Metropolis algorithm is that it provides posterior distributions of retrieved variables, which present a detailed picture of the behavior and uncertainty of individual variables, conditioned on both the model and the observed data. Therefore the retrieved distributions provide information about the parameter sensitivity of the PROSAIL-2 model. For simplicity, we have grouped variable behavior into three major categories: well-constrained, edge-hitting and poorly-constrained (Braswell et al., 2005). The "well-constrained" variables usually have a well-defined distribution, with small standard deviations relative to their allowable ranges. The "poorly-constrained" variables have relatively flat distributions with large standard deviations relative to their allowable ranges. Edge-hitting variables are those for which the modes of their retrieved values occurred near one of the edges of their

Table 2
Posterior means, standard deviations, variable behavior from inversion of the PROSAIL-2 model with the three simulated data sets: no data error, noise standard deviation $\sigma = 5\%$*data, noise standard deviation $\sigma = 10\%$*data

Variable	Actual	No error		$\sigma = 5\%$*data		$\sigma = 10\%$*data	
		Mean ± standard deviation	Variable class	Mean ± standard deviation	Variable class	Mean ± standard deviation	Variable class
PAI	4.5	4.43 ± 1.25	Well-constrained	4.42 ± 1.29	Well-constrained	4.57 ± 1.33	Well-constrained
SFRAC	0.1	0.102 ± 0.070	Well-constrained	0.090 ± 0.070	Well-constrained	0.088 ± 0.070	Well-constrained
CF	0.9	0.88 ± 0.09	Well-constrained	0.87 ± 0.11	Well-constrained	0.87 ± 0.14	Well-constrained
C_{ab}	35.0	36.36 ± 8.89	Well-constrained	37.0 ± 8.91	Well-constrained	36.61 ± 9.16	Well-constrained
N	1.5	1.43 ± 0.19	Well-constrained	1.43 ± 0.19	Well-constrained	1.42 ± 0.19	Well-constrained
C_w	0.03	0.0327 ± 0.0087	Well-constrained	0.0328 ± 0.0084	Well-constrained	0.033 ± 0.0086	Well-constrained
C_m	0.01	0.0109 ± 0.007	Well-constrained	0.0115 ± 0.007	Well-constrained	0.0115 ± 0.0068	Well-constrained
C_{brown}	0.7	0.7000 ± 0.240	Well-constrained	0.7264 ± 0.246	Well-constrained	0.7346 ± 0.243	Well-constrained
LFINC	45.0	41.69 ± 8.36	Well-constrained	42.20 ± 8.37	Well-constrained	41.40 ± 8.50	Well-constrained
STINC	50.0	43.51 ± 21.84	Poorly-constrained	43.54 ± 22.15	Poorly-constrained	43.28 ± 22.04	Poorly-constrained
LFHOT	0.05	0.1896 ± 0.1998	Edge-hitting	0.1784 ± 0.1844	Edge-hitting	0.2021 ± 0.2108	Edge-hitting
STHOT	0.05	0.3982 ± 0.2575	Poorly-constrained	0.4074 ± 0.2552	Poorly-constrained	0.4156 ± 0.2598	Poorly-constrained
$STEM_A$	10.0	9.7928 ± 5.7782	Poorly-constrained	9.7494 ± 5.7937	Poorly-constrained	9.7993 ± 5.7817	Poorly-constrained
$STEM_B$	2820	3025 ± 1210	Poorly-constrained	3061 ± 1207	Poorly-constrained	3014 ± 1222	Poorly-constrained
$SOIL_A$	10.0	9.9686 ± 5.8055	Poorly-constrained	9.8590 ± 5.6977	Poorly-constrained	9.9686 ± 5.8054	Poorly-constrained
$SOIL_B$	3525	3204 ± 1139	Poorly-constrained	3205 ± 1123	Poorly-constrained	3149 ± 1148	Poorly-constrained
$FAPAR_{canopy}$	0.84	0.84 ± 0.10	Well-constrained	0.83 ± 0.11	Well-constrained	0.83 ± 0.11	Well-constrained
$FAPAR_{leaf}$	0.76	0.76 ± 0.11	Well-constrained	0.74 ± 0.12	Well-constrained	0.73 ± 0.11	Well-constrained
$FAPAR_{chl}$	0.59	0.58 ± 0.11	Well-constrained	0.56 ± 0.13	Well-constrained	0.56 ± 0.14	Well-constrained

allowable ranges and most of the retrieved values were clustered near this edge. As shown in Table 2, among the 16 biophysical/biochemical variables in the PROSAIL-2 model, nine variables had "well-constrained" distributions, six variables had "poorly-constrained" distributions, and one variable had "edge-hitting" distribution. By forward calculation with the retrieved distributions, we found that $FAPAR_{canopy}$, $FAPAR_{leaf}$ and $FAPAR_{chl}$ were also "well-constrained". Because of page limits we did not present the graphs to show the histograms of individual variables from the simulated data. Graphs showing the histograms of individual variables retrieved from the MODIS data (see Section 3.2) illustrate the variable behaviors we discussed in this section.

3. Description of the Harvard Forest site and multiple daily MODIS data collections

3.1. Brief description of the Harvard Forest site

The Harvard Forest eddy flux tower site (42.54°N and 72.18°W, 180–490 m elevation) is located in western Massachusetts, USA. The vegetation is primarily deciduous broadleaf forest, dominated by red oak (*Quercus rubra*), red maple (*Acer rubrum*), black birch (*Betula lenta*) and white pine (*Pinus strobus*). There are also some evergreen needleleaf species within the forest, for example, eastern hemlock (*Tsuga canadensis*) (Waring et al., 1995). Altogether, deciduous broadleaf forest occupies 56% of the land, conifer forest occupies 12%, and mixed forest occupies 20% (Turner et al., 2003). The canopy height is approximately 20–24 m. Soils are mainly sandy loam glacial till with some alluvial and colluvial deposits. The climate is cool, moist temperate with July mean temperature 20 °C. Annual mean precipitation is about 110 cm, and the precipitation is distributed approximately evenly throughout the year. Most areas are at least moderately well drained (Barford et al., 2001; Goulden et al., 1996; Wofsy et al., 1993). The major deciduous species of Harvard Forest commenced senescence on about September 17th in 1991 and 1992 (Bassow & Bazzaz, 1998). Intensive fieldwork has been conducted at the site for measuring leaf chlorophyll content by species (Waring et al., 1995) and LAI (Cohen et al., 2003; Xiao et al., 2004b). These field data are useful and available for evaluating estimated values of chlorophyll content and LAI from inversion of the PROSAIL-2 model.

3.2. Collection of multiple daily MODIS data over the Harvard Forest site

Three MODIS standard products are used in this study: MODIS daily surface reflectance (MOD09GHK, v004), MODIS daily observation viewing geometry (MODMGGAD, v004), and MODIS daily observation pointers (MODPTHKM, v004). The MODIS daily surface reflectance product has surface reflectance values of seven spectral bands (500m spatial resolution) that are primarily designed for study of vegetation and land surface: red (620–670 nm), blue (459–479 nm), green (545–565 nm), near infrared (NIR_1, 841–875 nm, and NIR_2, 1230–1250 nm), short-wave infrared ($SWIR_1$, 1628–1652 nm, and $SWIR_2$, 2105–2155 nm). The MODIS daily observation viewing geometry product contains observation viewing geometry information (view zenith angle, view azimuth angle, sun zenith angle and sun azimuth angle) at a nominal 1-km scale. The MODIS daily observation pointers product provides a reference, at the 500 m scale, to observations that intersect each pixel of MODIS daily surface reflectance product in MODIS daily observation viewing geometry product (personal

Table 3
A list of MODIS multiple daily data collections in 2001 through 2003 for inversion of the PROSAIL-2 model; DOY—day of year

Year	DOY period	Number of valid observations
2001	201–214	17
	250–260	13
2002	147–162	10
	219–230	10
2003	172–187	13
	248–255	13

communication with Dr. Robert Wolfe). All these three MODIS data products are freely available at USGS EROS Data Center (http://www.edc.usgs.gov/).

The quality control (QC) data layer from the MODIS daily surface reflectance product includes information about errors and missing data in the daily surface reflectance product, for each of the seven MODIS bands, as well as information about whether an atmospheric correction was performed, and information about whether an adjacency correction was performed. If the QC value indicates any quality problem, the observation was not used in our analysis. In addition, we tried to avoid residual cloud-contaminated observations by carefully screening reflectance values of the MODIS blue band (459–479 nm). The reflectance of forested and other vegetated areas is generally less than 0.05 (Kaufman et al., 1997) under cloud-free conditions. If the MODIS blue band reflectance is greater than 0.05, and the QC flag indicates no quality problem, the observation is still excluded from the analysis. In addition, the blue band is very sensitive to residual aerosol, and the $SWIR_2$ band is very sensitive to subpixel water bodies (King et al., 1999). Therefore, both the blue and $SWIR_2$ bands were not used for inversion of PROSAIL-2 model. In this study, we used information from the other five MODIS bands to invert PROSAIL-2 model. Thus, in Eqs. (1) and (2), p is equal to five, $X_i=[x_{i1},x_{i2},x_{i3},x_{i4},x_{i5}]'$, and $U_i=[u_{i1},u_{i2},u_{i3},u_{i4},u_{i5}]$, where subscripts 1, 2, 3, 4, 5 refer to red, NIR_1, green, NIR_2, and $SWIR_1$ bands of MODIS, respectively.

We acquired daily MODIS data (year 2001 through year 2003) from the NASA data archive, for an area containing the Harvard Forest site. To invert all the sixteen variables of the PROSAIL-2 model simultaneously with daily MODIS data, one needs to have sufficient satellite observations of adequate quality. For the MODIS sensor onboard the Terra satellite, there are not enough satellite observations over Harvard Forest site within 1 day to allow a stable inversion of the PROSAIL-2 model (the problem is underdetermined). One solution is to

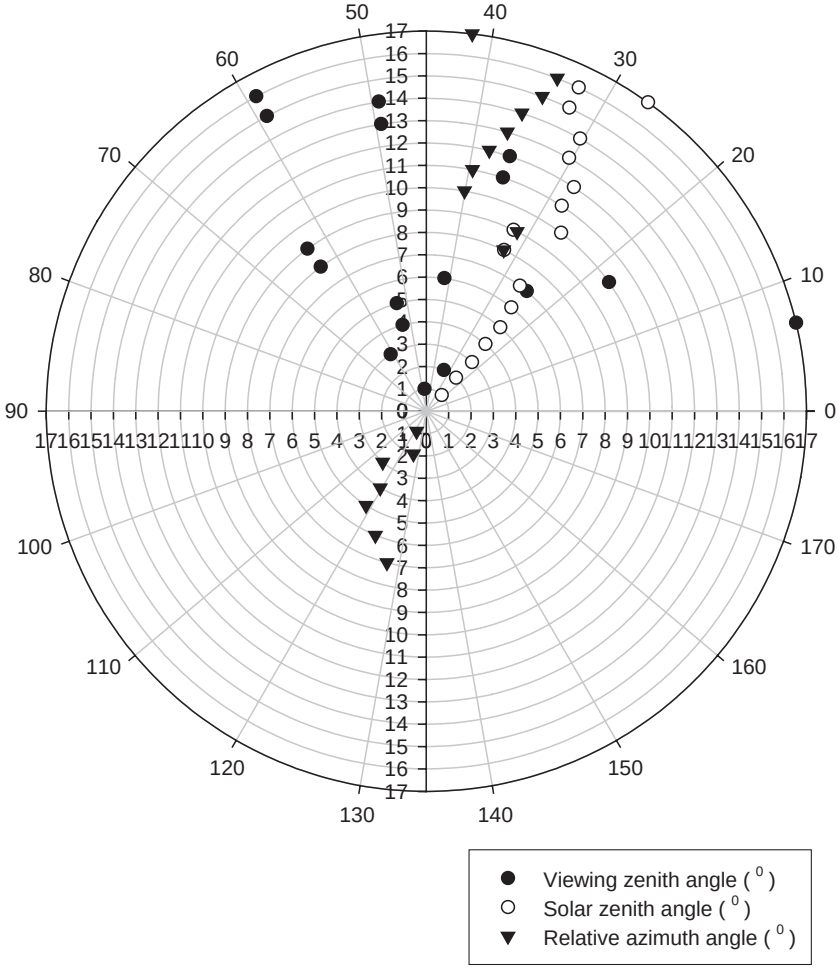

Fig. 1. Viewing geometries of data collection from DOY 201–214 in 2001 (17 observations).

collect satellite observations over a longer period of time, for example, over a 16 days period as is done in the production of the standard MODIS nadir-adjusted product (MOD43; Strahler et al., 1999). To balance the need for many satellite observations and the need for collecting observations over a short period of time, we used a flexible scheme for organizing observations for inversion of the PROSAIL-2 model (Table 3). We assumed that there is negligible variation of the canopy and the leaf within the period of each data collection in Table 3. This assumption is commonly used when researchers need many observations during a short period (e.g., Strahler et al., 1999). Each of the six data collections in Table 3 has 10–17 good-quality observations and covers no more than sixteen consecutive days. The MODIS observations associated with the individual data collections have large variations in observation geometry. For example, Fig. 1 shows the variation of observation geometry for the data collection from DOY 201–214 in 2001.

3.3. Inversion of the PROSAIL-2 model with MODIS data

For this paper, we designed an inversion scheme to estimate the sixteen biophysical and biochemical variables using observed spectral reflectance data. We performed inversions of the PROSAIL-2 model for each of the six data collections using the Metropolis algorithm, resulting in the distributions of individual variables for each data collection. We evaluated the inversions of the PROSAIL-2 model in three ways. First, we compared observed surface reflectance from the MODIS image with surface reflectance retrieved using PROSAIL-2. For the

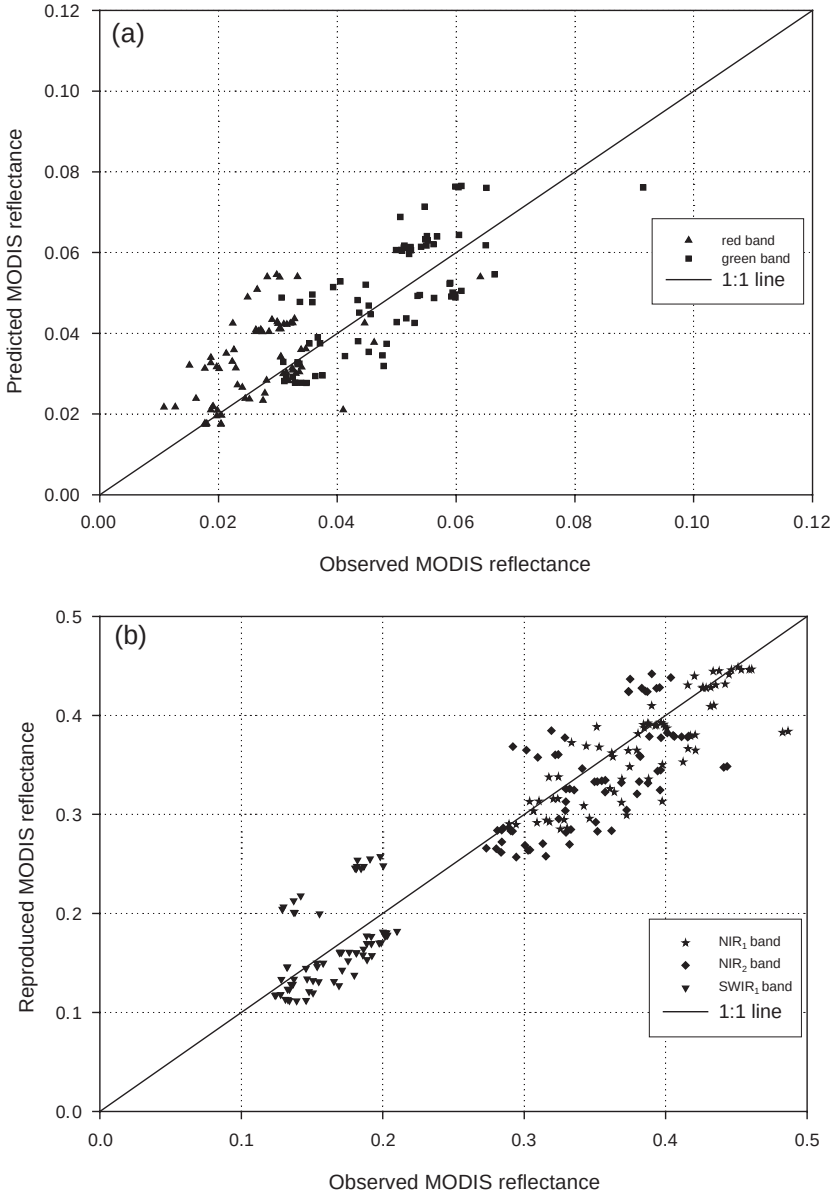

Fig. 2. A comparison between the observed reflectance and PROSAIL-2-reproduced reflectance for five MODIS spectral bands (red, green, NIR_1, NIR_2 and $SWIR_1$). Surface reflectances were reproduced with the mean values of inverted variables from the PROSAIL-2 model in 2001, 2002 and 2003. (a) MODIS red and green bands and (b) MODIS NIR_1, NIR_2, and $SWIR_1$ spectral bands.

Table 4
Variable behavior from inversion of the PROSAIL-2 model with the MODIS data collection from DOY 147–162 in 2002

Variable	Variable behavior
PAI	Well-constrained
SFRAC	Well-constrained
CF	Edge-hitting
C_{ab}	Well-constrained
N	Well-constrained
C_w	Well-constrained
C_m	Well-constrained
C_{brown}	Well-constrained
LFINC	Well-constrained
STINC	Poorly-constrained
LFHOT	Well-constrained
STHOT	Poorly-constrained
$STEM_A$	Poorly-constrained
$STEM_B$	Poorly-constrained
$SOIL_A$	Poorly-constrained
$SOIL_B$	Poorly-constrained
$FAPAR_{canopy}$	Well-constrained
$FAPAR_{leaf}$	Well-constrained
$FAPAR_{chl}$	Well-constrained

forward calculations of reflectance we used the mean values of variables taken from the posterior distributions. Secondly, we examined the temporal variations of a few key variables from inversion of the PROSAIL-2 model, with available data about LAI and chlorophyll content from the literature. Thirdly, we examined the temporal variation of $FAPAR_{canopy}$, $FAPAR_{leaf}$ and $FAPAR_{chl}$, and compared them with two commonly used vegetation indices, NDVI and the Enhanced Vegetation Index (EVI, Huete et al., 1997), showing their temporal patterns and magnitudes with respect to FAPAR values.

$$\mathrm{NDVI} = \frac{\rho_{\mathrm{NIR}_1} - \rho_{\mathrm{red}}}{\rho_{\mathrm{NIR}_1} + \rho_{\mathrm{red}}} \tag{10}$$

$$\mathrm{EVI} = 2.5 \times \frac{\rho_{\mathrm{NIR}_1} - \rho_{\mathrm{red}}}{\rho_{\mathrm{NIR}_1} + 6 \times \rho_{\mathrm{red}} - 7.5 \times \rho_{\mathrm{blue}} + 1} \tag{11}$$

where ρ_{blue}, ρ_{red} and ρ_{NIR_1} are reflectance values of the blue, red and NIR_1 bands.

4. Results

4.1. Comparison between retrieved and observed reflectance values

After the inversions of the PROSAIL-2 model, we utilized the mean values of the retrieved variable distributions for each data collection as inputs to calculate the reflectance with forward simulations of the PROSAIL-2 model. Fig. 2 shows a comparison of PROSAIL-2 retrieved reflectance with observed reflectance of MODIS green, red, NIR_1, NIR_2, and SWIR_1 bands. The correlation coefficient between retrieved and observed MODIS visible reflectance is 0.75 for green band and 0.54 for red band. The root mean squared error (RMSE) between observed and retrieved MODIS visible reflectance is 0.9% for green band and 0.9% for red band. The correlation coefficient between retrieved and observed NIR/SWIR reflectance is 0.83, 0.67, and 0.50 for NIR_1, NIR_2 and SWIR_1, respectively. The RMSE between observed and retrieved NIR/SWIR reflectance is 2.8%, 4.0%, and 3.7% for NIR_1, NIR_2 and SWIR_1, respectively. Note that each data collection spanned approximately 2 weeks, and any variation of leaf and canopy during the period may have contributed to the discrepancies between our retrieved reflectance and MODIS observed reflectance. Possible errors introduced during MODIS preprocessing may also contribute to the discrepancies (e.g. imperfect atmospheric correction). The comparison suggests that PROSAIL-2 model with the retrieved mean values of individual variables reasonably reproduces the surface reflectance of the deciduous broadleaf forest site in 2001–2003.

4.2. Temporal variation of eight variables (PAI, SFRAC, CF, C_{ab}, N, C_w, C_m, C_{brown}) in the PROSAIL-2 model

The strength of the Metropolis inversion algorithm is that it estimates probability distributions for individual model variables. Inspection of these posterior distributions offers a measure of uncertainty in the form of their standard deviations or other quantile intervals. As discussed previously, the shape of the distributions provides a measure of compatibility between model and data. We examined the histograms of the sixteen variables from inversion of each MODIS data collection, and ranked them into the categories of "well-constrained", "poorly-constrained" and "edge-hitting". For the MODIS data collection in DOY 147–162, nine variables belong to "well-constrained", six variables to "poor-constrained" and one variable to "edge-hitting" (Table 4). For example, leaf chlorophyll content (C_{ab}) has a bell-shaped "well-constrained" distribution (Fig. 3), with a mean value of 35.9 μg/cm^2 and a standard deviation of 5.6 μg/cm^2. Stem fraction (SFRAC) has a relatively "well-constrained" distribution (Fig. 4) with a mean value of 8.8% and a standard deviation of 5.6%. In comparison, cover fraction (CF) has a distribution that clearly belongs to the "edge-hitting" category (Fig. 5), with a mean value of 92% and a standard deviation of

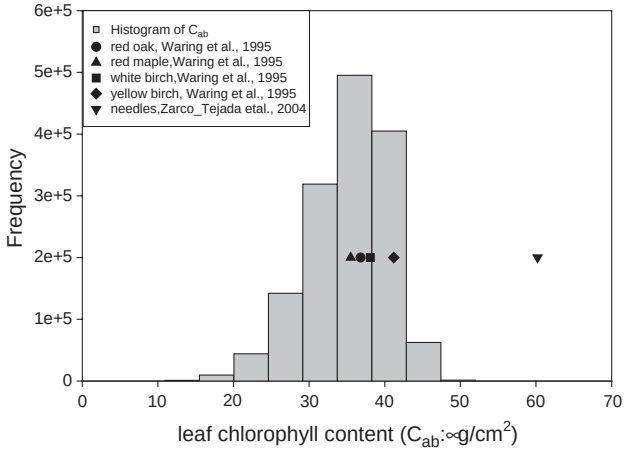

Fig. 3. Histogram of leaf chlorophyll content (C_{ab}, μg/cm^2) for MODIS data collection from DOY 147–162 in 2002.

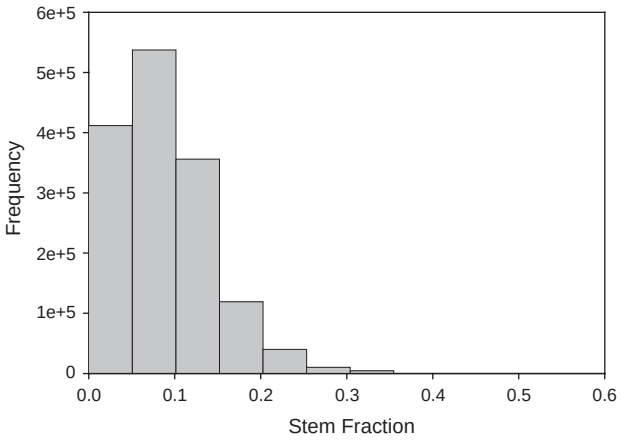

Fig. 4. Histogram of stem fraction for MODIS data collection from DOY 147–162 in 2002.

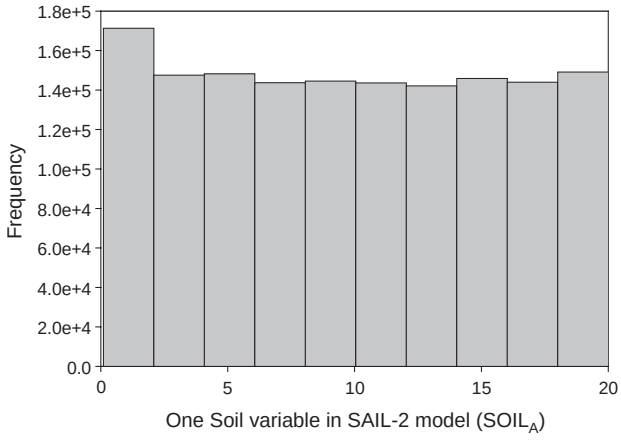

Fig. 6. Histogram of one soil parameter in SAIL-2 ($SOIL_A$) for MODIS data collection from DOY 147–162 in 2002.

7%. The soil variable ($SOIL_A$) is "poorly-constrained" (Fig. 6) and has a mean value of 9.94 and a standard deviation of 5.79. We calculated LAI, based on estimated values of PAI and SFRAC, and we see that its resultant distribution is "well constrained" (Fig. 7) with a mean value of 4.2 and a standard deviation of 1.3. For the other five MODIS data collections, the results were similar. Both stem and soil variables contributed relatively little to surface reflectance, largely due to a very high percentage of forest cover and large values (4.9 in peak growing season of 2001) of leaf area index in the Harvard Forest site (Cohen et al., 2003).

Fig. 8 shows the temporal variation of the mean and standard deviation of three canopy-level variables in the PROSAIL-2 model. The mean value of plant area index (PAI) from DOY 147–260 in 2001–2003 varies between 4 and 5 (Fig. 8a), with a slightly increasing tendency of PAI from DOY 147–210, and a slightly decreasing tendency of PAI from DOY 230 to DOY 260. The mean value of stem fraction from DOY 147–260 in 2001–2003 was within the range of about 2–10%, and the data collection from DOY 147–162 in 2002 had the largest value of stem fraction among the six data collections (Fig. 8b). Stem fraction explained why the difference between the mean value of $FAPAR_{canopy}$ and the mean value of $FAPAR_{leaf}$ of the data collection from DOY 147–162 in 2002 was the greatest among all the six data collections (Fig. 10a). The mean value of cover fraction from DOY 147–260 in 2001–2003 was within the range of 92–99%, and the data collection from DOY 147–162 in 2002 had the smallest value of cover fraction among the six data collections (Fig. 8c). The cover fraction histogram of the data collection from DOY 147–162 in 2002 is shown in Fig. 5. Its mode appears near the right edge of its allowable range (Table 1). All other modes of cover fraction for the six data collections also appear near the right edge. This is why some of the "mean plus standard deviation" values are greater than 1.0 in Fig. 8c. We calculated LAI using the equation $LAI=(1-SFRAC)\times PAI$. The resultant LAI mean values vary between 3.9 in DOY 147–162 in 2002 and 4.4 in DOY 201–214 in 2001 (Fig. 8d).

Fig. 9 shows the temporal variation of the mean and standard deviation of the five leaf-level variables in the PROSAIL-2 model. At leaf level, the estimated mean leaf chlorophyll content (C_{ab}) among the six data collections ranges from 35.9 to 51.7 μg/cm^2. The C_{ab} content of the data collection from DOY 147–162 in 2002 is the lowest retrieved value, and is

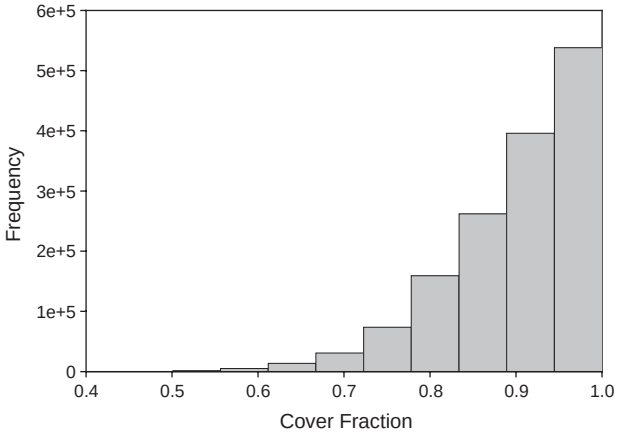

Fig. 5. Histogram of cover fraction for MODIS data collection from DOY 147–162 in 2002.

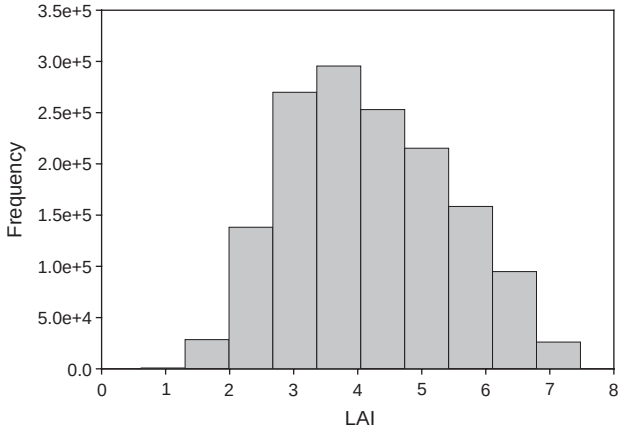

Fig. 7. Histogram of leaf area index (LAI) for MODIS data collection from DOY 147–162 in 2002.

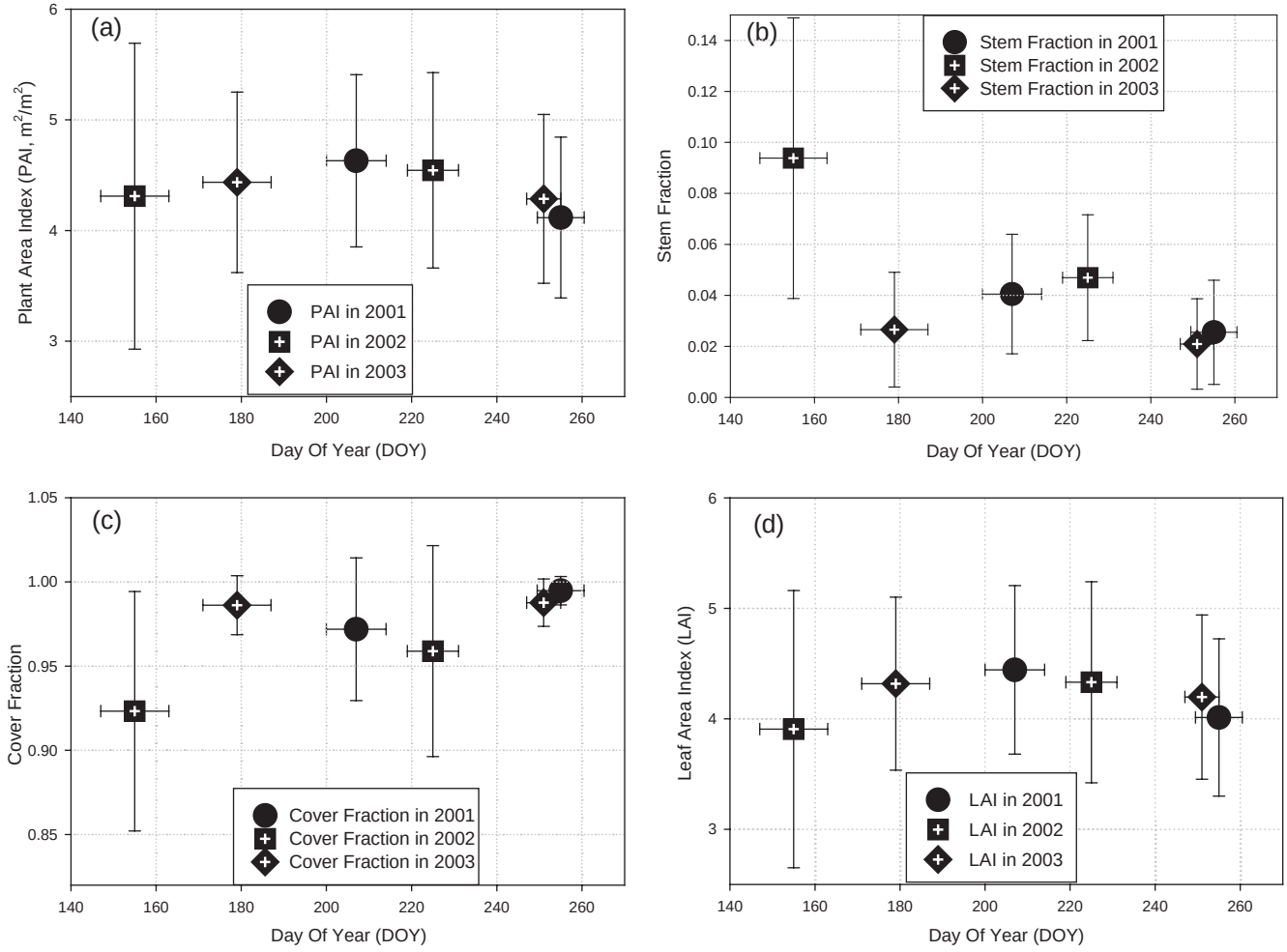

Fig. 8. Temporal variation of canopy-level variables from inversion of PROSAIL-2 model and LAI at Harvard Forest in 2001, 2002 and 2003. (a) Plant Area Index (PAI); (b) Stem Fraction; (c) Cover Fraction; and (d) leaf area index (LAI).

statistically different from the other five data collections. The mean values of C_{ab} content for the five data collections from DOY 172–260 have only a slight variation, well within the range of 10% (Fig. 9a). Leaf brown pigment (C_{brown}) shows a distinct seasonality with an increasing tendency from DOY 150 to DOY 260 (Fig. 9b). The data collection from DOY 172–187 in 2003 had the lowest mean value of leaf dry matter (C_m), which is significantly different from the other five collections. The mean values of C_m vary between 0.009 and 0.015 g/m^2 among the other five data collections (Fig. 9c). The structural variable of leaf (N) had a distinct seasonality with an increasing tendency from DOY 147–260 (Fig. 9d). Leaf equivalent water thickness (C_w) ranged between 0.015 cm and 0.032 cm, with a distinct temporal variation (Fig. 9e).

4.3. Temporal variation of $FAPAR_{canopy}$, $FAPAR_{leaf}$, and $FAPAR_{chl}$

We estimated the distributions of $FAPAR_{canopy}$, $FAPAR_{leaf}$, and $FAPAR_{chl}$ for each data collection, and extracted their mean and standard deviation (Fig. 10). The maximum mean values of $FAPAR_{canopy}$, $FAPAR_{leaf}$, and $FAPAR_{chl}$ were 0.92, 0.90, and 0.74, respectively. The minimum mean values were 0.83, 0.74, and 0.57, respectively. The ratios of minimum value to maximum value, a quantitative indicator of data dispersion, were 0.91, 0.83, and 0.77, respectively. $FAPAR_{canopy}$, $FAPAR_{leaf}$, and $FAPAR_{chl}$ exhibited different magnitudes of temporal variations, with $FAPAR_{canopy}$ and $FAPAR_{leaf}$ showing only slight changes throughout the peak growing season from DOY 172 to DOY 260, and $FAPAR_{chl}$ showing a strong seasonal variation.

The difference between $FAPAR_{canopy}$ and $FAPAR_{leaf}$ is attributed to light absorption by stem ($APAR_{stem}$), i.e., the non-leaf part of the canopy. During the peak growing season (mid-June to mid-September), the vegetation canopy is dominated by leaves, and only a very small proportion of stems are observed by the MODIS sensor. This may explain why $FAPAR_{canopy}$ values are only slightly higher than $FAPAR_{leaf}$ for the five data collections from DOY 172–260 (Fig. 10a). In comparison, $FAPAR_{canopy}$ in DOY147–162 in 2002 is much larger than $FAPAR_{leaf}$, which is likely to be due to a slightly higher proportion of stems observed by the MODIS sensor.

The difference between $FAPAR_{leaf}$ and $FAPAR_{chl}$ is attributed to light absorption by the non-chlorophyll component of the leaf. $FAPAR_{chl}$ values are substantially lower

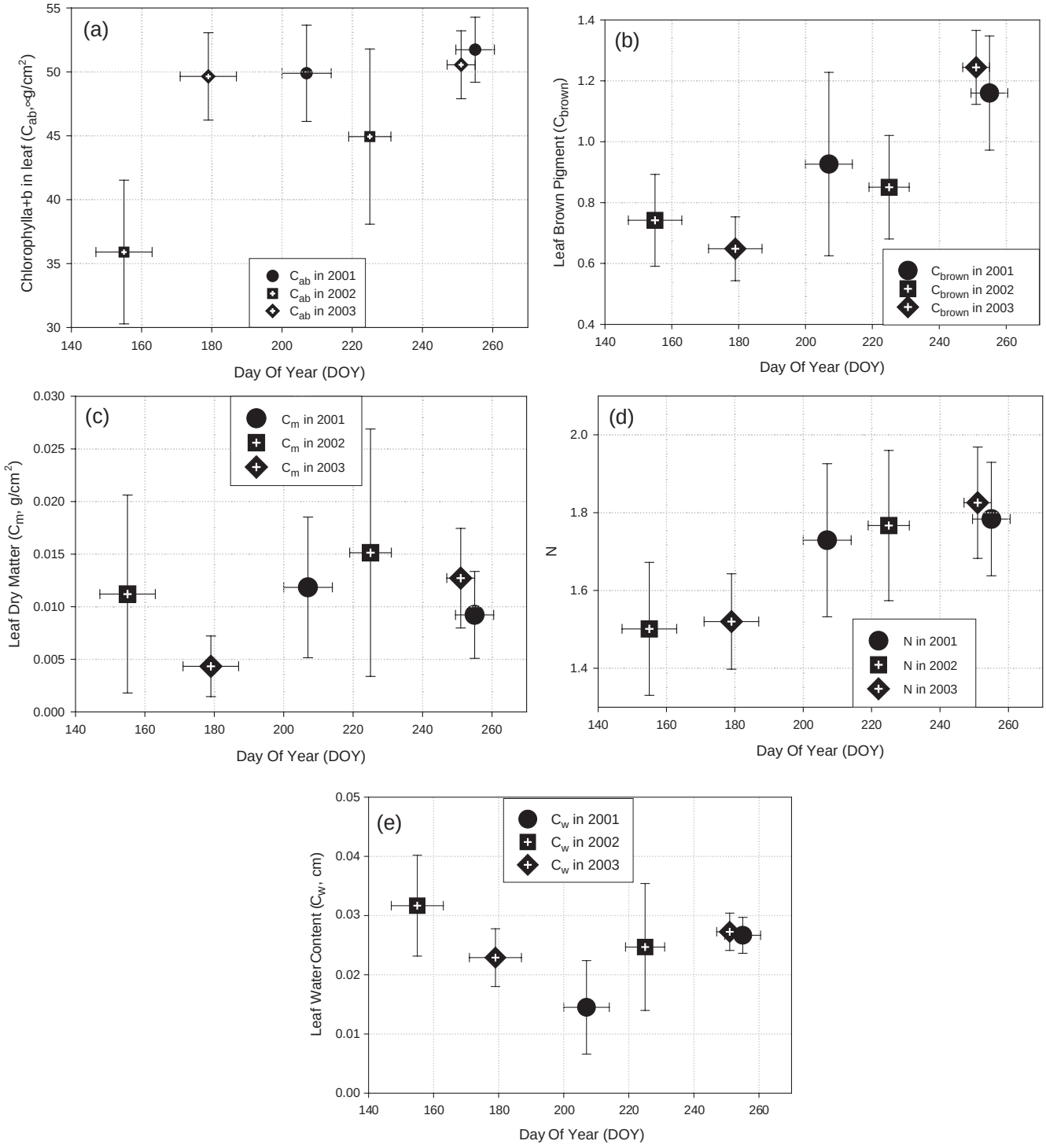

Fig. 9. Temporal variation of leaf-level variables from inversion of PROSAIL-2 model at Harvard Forest in 2001, 2002 and 2003; (a) leaf chlorophyll content (C_{ab}, μg/cm^2), (b) leaf brown pigment (C_{brown}), (c) leaf dry matter (C_m, g/cm^2), (d) N (structural parameter of leaf), and (e) leaf equivalent water thickness (C_w, cm).

than $FAPAR_{leaf}$ (Fig. 10a). Furthermore, the difference between $FAPAR_{leaf}$ and $FAPAR_{chl}$ increased over time from DOY 172 to DOY 260 (Fig. 10a), which is attributed to increases of light absorption by NPV components within the leaves. This suggests that leaf age and associated changes in dry matter and brown pigment components may affect the proportions of light absorption by NPV in the leaf and by chlorophyll.

NDVI has been widely used for estimation of $FAPAR_{canopy}$ and GPP. In recent years, EVI has been used frequently as well (Justice et al., 1998). We calculated the mean and standard deviation of NDVI and EVI using the same MODIS images for each data collection.

For the five data collections from DOY 172 to DOY 260, mean NDVI values are very similar to $FAPAR_{leaf}$ (Fig. 10b), which supports the earlier studies that used NDVI to

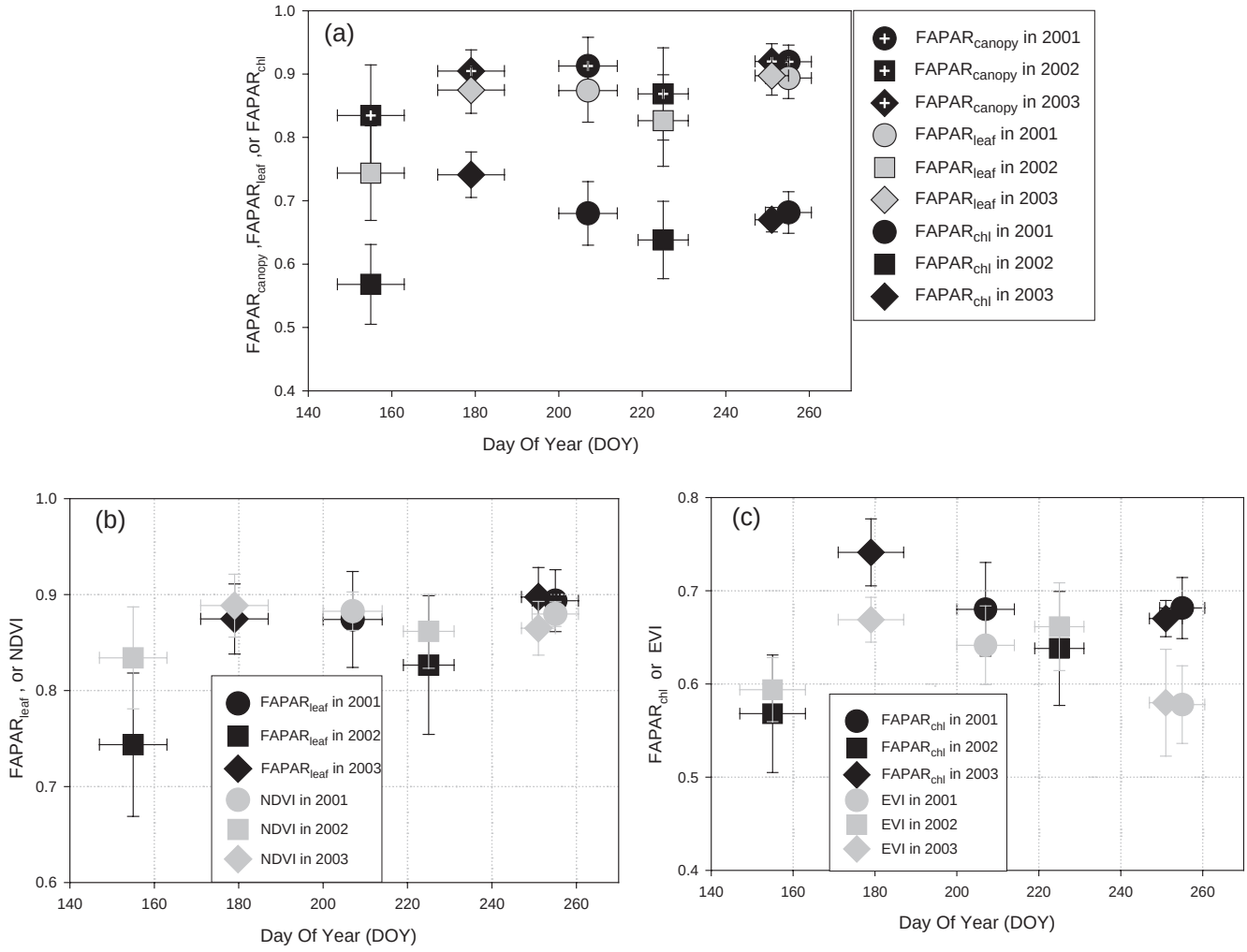

Fig. 10. Temporal variations of the fraction of photosynthetically active radiation absorbed by chlorophyll, leaf and canopy, and vegetation indices at Harvard Forest in 2001, 2002, 2003. (a) A comparison of estimated FAPAR$_{canopy}$, FAPAR$_{leaf}$ and FAPAR$_{chl}$; (b) a comparison between estimated FAPAR$_{leaf}$ and NDVI; and (c) a comparison between estimated FAPAR$_{chl}$ and EVI.

approximate FAPAR$_{canopy}$ (e.g., Goward et al., 1992), as FAPAR$_{leaf}$ and FAPAR$_{canopy}$ values are close to each other in those five data collections. However, the NDVI associated with the data collection from DOY 147–162 in 2002 is much greater than FAPAR$_{leaf}$, but close to FAPAR$_{canopy}$ (Fig. 10b). In general, mean EVI values vary substantially over time and are much closer to FAPAR$_{chl}$ values than mean NDVI values (Fig. 10c). Note that reflectance values in daily MODIS images are not BRDF corrected reflectance; therefore, the observation viewing geometry has an effect on the dynamics of NDVI and EVI. The standard deviation of EVI varies among the six data collections. For example, the EVI from DOY 248–255 in 2003 has a standard deviation of 0.057 (about 10% of mean EVI value). Therefore, caution should be taken when selecting daily MODIS images to calculate vegetation indices for use in estimation of FAPAR$_{canopy}$ and FAPAR$_{chl}$.

5. Discussion

Satellite-based optical sensors provide daily observations of the land surface at moderate spatial resolution. Numerous studies have used various radiative transfer models (RTM) to retrieve LAI and estimate FAPAR$_{canopy}$ (e.g., Asner et al., 1998; Bicheron & Leroy, 1999; Myneni et al., 1997). The MODIS Land Science Team has used a 3-dimentional radiative transfer model to provide standard products of FARAR$_{canopy}$ and LAI at 1 km spatial resolution (Justice et al., 1998; Knyazikhin et al., 1998). In this study we used a relatively simple RTM (PROSAIL-2 model) to study light absorption by chlorophyll, leaf and canopy over time. Our modified version of the PROSAIL-2 based inversion includes brown pigments for better characterization of leaf absorption, and the Metropolis inversion algorithm for estimation of variable uncertainties and model-data compatibility.

There is currently a paucity of in situ independent data for evaluation of retrieved LAI and FAPAR$_{canopy}$ at moderate (500 m to 1 km) spatial resolution (e.g., Cohen et al., 2003; Turner et al., 2003). Though field-based analyses are currently underway, we have no field-based data of chlorophyll, leaf water content and leaf dry matter in 2001–2003. In addition, the scaling problems associated with translating leaf chlorophyll to an image pixel at 500 m spatial resolution have yet to be

addressed. Here we discuss two variables (LAI and chlorophyll content) that are important for interpreting the results of inversion of the PROSAIL-2 model in this study.

LAI is an important canopy-level biophysical variable. In an effort to evaluate the standard product of LAI and $FAPAR_{canopy}$ from the MODIS Land Science Team, the BigFoot project was funded to study the spatial variation of LAI through a combination of extensive field sampling and Landsat images across a number of sites in North America. As part of the BigFoot project, the field study (Cohen et al., 2003) estimated spatial distributions of LAI at Harvard Forest and reported an LAI value of 4.9 during its mid growing season in 2001. Field researchers at Harvard Forest also conducted multi-temporal measurements of LAI in 1998 and 1999, which ranged from 3.4 to 4.2 in June–September of 1998, and from 3.8 to 4.7 in June–September of 1999 (Xiao et al., 2004b). Our estimated LAI mean values are within the range of LAI measured in 1998–1999 (Figs. 7 and 8d). The MODIS standard LAI/FPAR product (MOD15A2, v004) estimates LAI values of >6.0 at the Harvard Forest during June–September of 2001–2003. In this study, estimated mean LAI value from inversion of the PROSAIL-2 model for the data collection from DOY 201–214 in 2001 is about 4.4 (Fig. 8d), which is more consistent with the field-based estimate from Cohen et al. (2003). The differences in LAI values between the MOD15A2 standard product and PROSAIL-2 based estimates in this study are often larger than 1 at the Harvard Forest. It is beyond the scope of this paper to diagnose the errors of either LAI algorithm in detail, but we note that the MOD15A2 estimate assumes constant standard leaf optical properties for deciduous broadleaf forests throughout the entire plant growing season (Myneni et al., 2002). For inversions of the PROSAIL-2 model in this study, we assume that leaf-level variables (e.g., brown pigments, leaf dry matter) change over time. The good agreement between PROSAIL-2-retrieved LAI and observed field LAI values suggests that inversions of the PROSAIL-2 model in this study work reasonably well.

Leaf chlorophyll content (C_{ab}) is an important biochemical variable and one of the major control factors of photosynthesis. Given light intensity and atmospheric CO_2 concentration, it has been reported that the chlorophyll content of red oak, one of the major species of Harvard Forest, would not change during the peak plant growing season prior to senescence (Cavender-Bares et al., 2000). Furthermore, there was no observed significant inter-annual change of chlorophyll content of the major species of Harvard Forest between 1995 and 1996 during plant growing periods before senescence (personal communication with Dr. Jeannine Cavender-Bares). The chlorophyll content of red oak at Harvard Forest in August of 1991 was measured to be 36.8 μg/cm^2, red maple 35.5 μg/cm^2, white birch 38.1 μg/cm^2, and yellow birch 41.2 μg/cm^2 (Waring et al., 1995). A research group recently reported that their measurement of chlorophyll content of needles in late July of 1998 and 1999 was 60.2 μg/cm^2 (Zarco-Tejada et al., 2004), which was higher than the reported values of chlorophyll content of hardwood species of Harvard Forest by other studies (Cavender-Bares et al., 2000; Waring et al., 1995). Needleleaf trees are distributed in parts of the Harvard Forest site. The chlorophyll content of Harvard Forest leaves at the MODIS scale (500 m) is therefore likely to fall between the hardwood and needleleaf values, dependent upon the mixing ratio of hardwood trees and needleleaf trees. In this study, the estimated mean C_{ab} value for the data collection from DOY 147–162 in 2002 was 35.9 μg/cm^2, and the estimated mean C_{ab} values for the other five data collections were 44.9–51.7 μg/cm^2. These C_{ab} estimates fall within the range between the C_{ab} of hardwood trees and C_{ab} of needles reported by other researchers. While measurement of leaf chlorophyll content at individual leaves is tractable, scaling measurements of individual leaves to a MODIS image pixel (500 m) represents a major leap requiring a rigorous field sampling design. The results of this study suggest that future fieldwork in deciduous broadleaf forests should include multi-temporal measurements of leaf-level variables (chlorophyll and other pigments, leaf dry matter and leaf water content).

The number of variables in the PROSAIL-2 model that can be reasonably inverted simultaneously is still an unresolved issue. An earlier model simulation study (Jacquemoud et al., 2000) argued that the leaf structure variable (N) should be held at a fixed value during inversion of the other variables. Their inversion was conducted for the spectral range from 430 nm to 880 nm. Another study (Zarco-Tejada et al., 2003) inverted N, C_m, and C_w with the other variables held constant, using a MODIS 8-day composite reflectance data (MOD09A1) and MODIS LAI data (MOD15A2). Inversion of the PROSAIL-2 in our study has a broader spectral range from 555 nm to 1640 nm. In this study, inversion of the PROSAIL-2 model estimates simultaneously both canopy-level variables (e.g., PAI) and leaf-level variables, using multiple daily MODIS data. To our knowledge, this is the first study that simultaneously retrieves both canopy- and leaf-level variables through inversion of the PROSAIL-2 model and multiple daily MODIS data. The results of this study have demonstrated the potential of the PROSAIL-2 model as a tool for quantifying biophysical and biochemical variables of vegetation at leaf- and canopy-levels over time.

The results of this study highlight the differences among $FAPAR_{canopy}$, $FAPAR_{leaf}$ and $FAPAR_{chl}$ over time for a deciduous broadleaf forest. The substantial difference between $FAPAR_{canopy}$ and $FAPAR_{chl}$ may have significant implication for those biogeochemical models that estimate light absorption, GPP, and NPP using satellite data. A number of satellite-based Production Efficiency Models (Potter et al., 1993; Prince & Goward, 1995; Ruimy et al., 1996; Running et al., 2004) use $FAPAR_{canopy}$ to estimate the amount of PAR absorbed by canopies.

6. Summary

This study has demonstrated the potential for combining radiative transfer modeling with a Bayesian parameter estimation scheme, utilizing real satellite data for estimating leaf- and canopy-level biophysical and biochemical properties of a deciduous broadleaf forest. We estimated the PROSAIL-2

model variables based on the surface reflectance of the five MODIS spectral bands (green, red, NIR_1, NIR_2 and $SWIR_1$). We also estimated the seasonal dynamics of FAPAR at canopy-, leaf- and chlorophyll-levels, respectively. Our results show that $FAPAR_{chl}$ and $FAPAR_{canopy}$ exhibit different behaviors for a deciduous broadleaf forest. This study represents our effort in using a radiative transfer model to partition canopy-level FAPAR into $FAPAR_{chl}$ and $FAPAR_{NPV}$, following previous studies that proposed the conceptual partitioning ($FAPAR_{canopy} = FAPAR_{chl} + FAPAR_{NPV}$) and showed the potential of $FAPAR_{chl}$ in improving the quantification of GPP for forests. This study is another step that enables us to go beyond the LAI-$FAPAR_{canopy}$-NDVI paradigm and explore the alternative chlorophyll-$FAPAR_{chl}$ approach that takes advantage of moderate resolution optical sensors (e.g. MODIS) in the era of the Earth Observing System. This study also suggests that both remote sensing and ecological research would benefit from season-long measurements of leaf-level variables (e.g., chlorophyll, other pigments, leaf dry matter, and leaf water content), in addition to measurements of canopy-level variables (e.g., LAI).

Acknowledgements

We thank Dr. Stephane Jacquemoud for kindly providing his PROSPECT model code. We thank Dr. John Aber and Dr. George Hurtt for their useful advice and support. We thank Dr. Robert Wolfe, and Dr. Eric Vermote for their useful suggestions to preprocess the MODIS daily data. We thank Dr. Jeannine Cavender-Bares for her useful information (unpublished data) about chlorophyll content of Harvard Forest. We also thank Mr. Stephen Boles and four anonymous reviewers for their comments and suggestions on the earlier version of the manuscript. The study was supported by NASA Earth System Science Graduate Fellowship (NGT5-30477 for Q. Zhang) and NASA Earth Observation System Interdisciplinary Science project (NAG5-10135).

References

Andrieu, B., Baret, F., Jacquemoud, S., Malthus, T., & Steven, M. (1997). Evaluation of an improved version of SAIL model for simulating bidirectional reflectance of sugar beet canopies. *Remote Sensing of Environment*, *60*, 247–257.

Asner, G. P., Wessman, C. A., & Archer, S. (1998). Scale dependence of absorption of photosynthetically active radiation in terrestrial ecosystems. *Ecological Applications*, *8*, 1003–1021.

Bacour, C., Jacquemoud, S., Leroy, M., Hautecoeur, O., Weiss, M., Prevot, L., et al. (2002). Reliability of the estimation of vegetation characteristics by inversion of three canopy reflectance models on airborne POLDER data. *Agronomie*, *22*, 555–565.

Badhwar, G. D., Verhoef, W., & Bunnik, N. J. J. (1985). Comparative-study of SUITS and SAIL canopy reflectance models. *Remote Sensing of Environment*, *17*, 179–195.

Baret, F., & Fourty, T. (1997). Radiometric estimates of nitrogen status in leaves and canopies. In G. Lemaire (Ed.), *Diagnosis of the nitrogen status in crops* (pp. 201–227). Berlin: Springer.

Barford, C. C., Wofsy, S. C., Goulden, M. L., Munger, J. W., Pyle, E. H., Urbanski, S. P., et al. (2001). Factors controlling long- and short-term sequestration of atmospheric CO_2 in a mid-latitude forest. *Science*, *294*, 1688–1691.

Bassow, S. L., & Bazzaz, F. A. (1998). How environmental conditions affect canopy leaf-level photosynthesis in four deciduous tree species. *Ecology*, *79*, 2660–2675.

Bicheron, P., & Leroy, M. (1999). A method of biophysical parameter retrieval at global scale by inversion of a vegetation reflectance model. *Remote Sensing of Environment*, *67*, 251–266.

Bishop, C. (1995). Neural networks for pattern recognition. New York: Oxford University Press.

Braswell, B. H., Schimel, D. S., Privette, J. L., Moore, B., Emery, W. J., Sulzman, E. W., et al. (1996). Extracting ecological and biophysical information from AVHRR optical data: An integrated algorithm based on inverse modeling. *Journal of Geophysical Research-Atmospheres*, *101*, 23335–23348.

Braswell, B. H., Sacks, W. J., Linder, E., & Schimel, D. S. (2005). Estimating diurnal to annual ecosystem parameters by synthesis of a carbon flux model with eddy covariance net ecosystem exchange observations. *Global Change Biology*, *11*, 335–355.

Cavender-Bares, J., Potts, M., Zacharias, E., & Bazzaz, F. A. (2000). Consequences of CO_2 and light interactions for leaf phenology, growth, and senescence in *Quercus rubra*. *Global Change Biology*, *6*, 877–887.

Cohen, W. B., Maiersperger, T. K., Yang, Z. Q., Gower, S. T., Turner, D. P., Ritts, W. D., et al. (2003). Comparisons of land cover and LAI estimates derived from ETM plus and MODIS for four sites in North America: a quality assessment of 2000/2001 provisional MODIS products. *Remote Sensing of Environment*, *88*, 233–255.

Combal, B., Baret, F., & Weiss, M. (2002). Improving canopy variables estimation from remote sensing data by exploiting ancillary information. Case study on sugar beet canopies. *Agronomie*, *22*, 205–215.

Demarez, V., Gastellu-Etchegorry, J. P., Mougin, E., Marty, G., Proisy, C., Dufrene, E., et al. (1999). Seasonal variation of leaf chlorophyll content of a temperate forest. Inversion of the PROSPECT model. *International Journal of Remote Sensing*, *20*, 879–894.

Depury, D. G. G., & Farquhar, G. D. (1997). Simple scaling of photosynthesis from leaves to canopies without the errors of big-leaf models. *Plant Cell and Environment*, *20*, 537–557.

Di Bella, C. M., Paruelo, J. M., Becerra, J. E., Bacour, C., & Baret, F. (2004). Effect of senescent leaves on NDVI-based estimates of f APAR: Experimental and modelling evidences. *International Journal of Remote Sensing*, *25*, 5415–5427.

Field, C. B., Randerson, J. T., & Malmstrom, C. M. (1995). Global net primary production—combining ecology and remote-sensing. *Remote Sensing of Environment*, *51*, 74–88.

Gelman, A., Carlin, J. B., Stern, H. S., & Rubin, D. B. (2000). Markov chain simulation (chapter 11). *Bayesian data analysis*. New York: Champman and Hall /CRC.

Goel, N. S., & Deering, D. W. (1985). Evaluation of a canopy reflectance model for LAI estimation through its inversion. *IEEE Transactions on Geoscience and Remote Sensing*, *23*, 674–684.

Goel, N. S., & Thompson, R. L. (1984). Inversion of vegetation canopy reflectance models for estimating agronomic variables: 5. Estimation of leaf-area index and average leaf angle using measured canopy reflectances. *Remote Sensing of Environment*, *16*, 69–85.

Gond, V., De Pury, D. G. G., Veroustraete, F., & Ceulemans, R. (1999). Seasonal variations in leaf area index, leaf chlorophyll, and water content; scaling-up to estimate fAPAR and carbon balance in a multilayer, multispecies temperate forest. *Tree Physiology*, *19*, 673–679.

Goulden, M. L., Munger, J. W., Fan, S. M., Daube, B. C., & Wofsy, S. C. (1996). Exchange of carbon dioxide by a deciduous forest: Response to interannual climate variability. *Science*, *271*, 1576–1578.

Goward, S. N., & Huemmrich, K. F. (1992). Vegetation canopy PAR absorptance and the normalized difference vegetation index—an assessment using the SAIL model. *Remote Sensing of Environment*, *39*, 119–140.

Hanan, N. P., Burba, G., Verma, S. B., Berry, J. A., Suyker, A., & Walter-Shea, E. A. (2002). Inversion of net ecosystem CO_2 flux measurements for estimation of canopy PAR absorption. *Global Change Biology*, *8*, 563–574.

Hanan, N. P., Kabat, P., Dolman, A. J., & Elbers, J. A. (1998). Photosynthesis and carbon balance of a Sahelian fallow savanna. *Global Change Biology*, *4*, 523–538.

Hosgood, B., Jacquemoud, S., Andreoli, G., Verdebout, J., Pedrini, G., & Schmuck, G. (1995). Leaf Optical Properties EXperiment 93 (LOPEX93). *European commision, joint research center, institute for remote sensing applications report EUR 16095 EN.*

Huete, A. R., Liu, H. Q., Batchily, K., & Vanleeuwen, W. (1997). A comparison of vegetation indices global set of TM images for EOS-MODIS. *Remote Sensing of Environment*, *59*, 440–451.

Hurtt, G. C., & Armstrong, R. A. (1996). A pelagic ecosystem model calibrated with BATS data. *Deep-Sea Research Part Ii-Topical Studies in Oceanography*, *43*, 653–683.

Jacquemoud, S., & Baret, F. (1990). PROSPECT—a model of leaf optical-properties spectra. *Remote Sensing of Environment*, *34*, 75–91.

Jacquemoud, S., Bacour, C., Poilve, H., & Frangi, J. P. (2000). Comparison of four radiative transfer models to simulate plant canopies reflectance: Direct and inverse mode. *Remote Sensing of Environment*, *74*, 471–481.

Jacquemoud, S., Ustin, S. L., Verdebout, J., Schmuck, G., Andreoli, G., & Hosgood, B. (1996). Estimating leaf biochemistry using the PROSPECT leaf optical properties model. *Remote Sensing of Environment*, *56*, 194–202.

Justice, C. O., Vermote, E., Townshend, J. R. G., Defries, R., Roy, D. P., Hall, D. K., et al. (1998). The Moderate Resolution Imaging Spectroradiometer (MODIS): Land remote sensing for global change research. *IEEE Transactions on Geoscience and Remote Sensing*, *36*, 1228–1249.

Kaufman, Y., Wald, A., Remer, L., Gao, B., Li, R., & Flynn, L. (1997). The MODIS 2.1-mm channel—Correlation with visible reflectance for use in remote sensing of aerosol. *IEEE Transactions on Geoscience and Remote Sensing*, *35*, 1286–1298.

King, M. D., Kaufman, Y. J., Tanre, D., & Nakajima, T. (1999). Remote sensing of tropospheric aerosols from space: Past, present, and future. *Bulletin of the American Meteorological Society*, *80*, 2229–2259.

Knyazikhin, Y., Martonchik, J. V., Myneni, R. B., Diner, D. J., & Running, S. W. (1998). Synergistic algorithm for estimating vegetation canopy leaf area index and fraction of absorbed photosynthetically active radiation from MODIS and MISR data. *Journal of Geophysical Research-Atmospheres*, *103*, 32257–32275.

Kuusk, A. (1985). The hotspot effect of a uniform vegetative cover. *Soviet Journal of Remote Sensing*, *3*, 645–658.

Lambers, H., Chapin, F. S., & Pons, T. L. (1998). *Plant physiological ecology*. New York: Spinger-Verlag.

Major, D. J., Schaalje, G. B., Wiegand, C., & Blad, B. L. (1992). Accuracy and sensitivity analyses of SAIL model-Predicted Reflectance of Maize. *Remote Sensing of Environment*, *41*, 61–70.

Metropolis, N., Rosenbluth, A. W., Rosenbluth, M. N., Teller, A. H., & Teller, E. (1953). Equations of state calculations by fast computing machines. *Journal of Chemical Physics*, *21*, 1087–1092.

Myneni, R. B., Nemani, R. R., & Running, S. W. (1997). Estimation of global leaf area index and absorbed PAR using radiative transfer models. *IEEE Transactions on Geoscience and Remote Sensing*, *35*, 1380–1393.

Myneni, R. B., Hoffman, S., Knyazikhin, Y., Privette, J. L., Glassy, J., Tian, Y., et al. (2002). Global products of vegetation leaf area and fraction absorbed PAR from year one of MODIS data. *Remote Sensing of Environment*, *83*, 214–231.

Newnham, G. J., & Burt, T. (2001). Validation of a leaf reflectance and transmittance model for three agricultural crop species. *International Geoscience and Remote Sensing Symposium*, *7*, 2976–2978.

Potter, C. S., Randerson, J. T., Field, C. B., Matson, P. A., Vitousek, P. M., Mooney, H. A., et al. (1993). Terrestrial ecosystem production—a process model-based on global satellite and surface data. *Global Biogeochemical Cycles*, *7*, 811–841.

Prince, S. D., & Goward, S. N. (1995). Global primary production: A remote sensing approach. *Journal of Biogeography*, *22*, 815–835.

Ruimy, A., Dedieu, G., & Saugier, B. (1996). TURC: A diagnostic model of continental gross primary productivity and net primary productivity. *Global Biogeochemical Cycles*, *10*, 269–285.

Ruimy, A., Kergoat, L., & Bondeau, A. (1999). Comparing global models of terrestrial net primary productivity (NPP): Analysis of differences in light absorption and light-use efficiency. *Global Change Biology*, *5*, 56–64.

Running, S., Nemani, R., Heinsch, F., Zhao, M., Reeves, M., & Hashimoto, H. (2004). A continuous satellite-derived measure of global terrestrial primary production. *Bioscience*, *54*, 547–560.

Strahler, A.H., Et Al. (1999). MODIS BRDF/Albedo Product: Algorithm Theoretical Basis Document, Version 5.0.

Tucker, C. J. (1979). Red and photographic infrared linear combinations for monitoring vegetation. *Remote Sensing of Environment*, *8*, 127–150.

Turner, D. P., Ritts, W. D., Cohen, W. B., Gower, S. T., Zhao, M. S., Running, S. W., et al. (2003). Scaling Gross Primary Production (GPP) over boreal and deciduous forest landscapes in support of MODIS GPP product validation. *Remote Sensing of Environment*, *88*, 256–270.

Verhoef, W. (1984). Light-scattering by leaf layers with application to canopy reflectance modeling—the SAIL model. *Remote Sensing of Environment*, *16*, 125–141.

Verhoef, W. (1985). Earth observation modeling based on layer scattering matrices. *Remote Sensing of Environment*, *17*, 165–178.

Verhoef, W., & Bach, H. (2003). Simulation of hyperspectral and directional radiance images using coupled biophysical and atmospheric radiative transfer models. *Remote Sensing of Environment*, *87*, 23–41.

Waring, R. H., Law, B. E., Goulden, M. L., Bassow, S. L., Mccreight, R. W., Wofsy, S. C., et al. (1995). Scaling gross ecosystem production at Harvard Forest with remote-sensing—a comparison of estimates from a constrained quantum-use efficiency model and eddy-correlation. *Plant Cell and Environment*, *18*, 1201–1213.

Weiss, M., Baret, F., Myneni, R. B., Pragnere, A., & Knyazikhin, Y. (2000). Investigation of a model inversion technique to estimate canopy biophysical variables from spectral and directional reflectance data. *Agronomie*, *20*, 3–22.

Wofsy, S. C., Goulden, M. L., Munger, J. W., Fan, S. M., Bakwin, P. S., Daube, B. C., et al. (1993). Net exchange of Co_2 in a midlatitude forest. *Science*, *260*, 1314–1317.

Xiao, X. M., Hollinger, D., Aber, J., Goltz, M., Davidson, E. A., Zhang, Q. Y., et al. (2004). Satellite-based modeling of gross primary production in an evergreen needleleaf forest. *Remote Sensing of Environment*, *89*, 519–534.

Xiao, X. M., Zhang, Q. Y., Braswell, B., Urbanski, S., Boles, S., Wofsy, S., et al. (2004). Modeling gross primary production of temperate deciduous broadleaf forest using satellite images and climate data. *Remote Sensing of Environment*, *91*, 256–270.

Zarco-Tejada, P. J., Miller, J. R., Harron, J., Hu, B. X., Noland, T. L., Goel, N., et al. (2004). Needle chlorophyll content estimation through model inversion using hyperspectral data from boreal conifer forest canopies. *Remote Sensing of Environment*, *89*, 189–199.

Zarco-Tejada, P. J., Rueda, C. A., & Ustin, S. L. (2003). Water content estimation in vegetation with MODIS reflectance data and model inversion methods. *Remote Sensing of Environment*, *85*, 109–124.